

Mesoscale Response to a Meandering Surface Temperature Interface

JOHN W. GLENDENING AND JAMES D. DOYLE

Marine Meteorology Division, Naval Research Laboratory, Monterey, California

(Manuscript received 22 April 1994, in final form 31 May 1994)

ABSTRACT

Mesoscale variation of the boundary-layer (BL) front produced by a surface temperature interface depends upon the scale of meander along that interface. For a relatively large-scale meander, the circulations are quasi two-dimensional relative to the local interface boundary, and a meander signature appears in the BL structure. For a relatively small-scale meander, alongfront blending eliminates organization about individual meanders to produce a quasi two-dimensional circulation and gradients oriented perpendicular to the mean front. The fundamental atmospheric scale controlling this transition is the mesoscale deformation radius, which depends upon the warm-side BL depth. With strong large-scale geostrophic forcing, however, the resulting alongfront advection length scale increases the meander size required to approach the large-scale limit. Large-scale meanders typically create two local maxima of vertical velocity, whereas small-scale meanders develop a single maximum on the warm side of the frontal zone. At intermediate scales, variations of the vertical velocity maximum are particularly complex when large-scale geostrophic winds are relatively weak.

1. Introduction

Abrupt changes in surface temperature produce mesoscale adjustments through their influence upon the atmospheric boundary layer (BL). The locus of maximum temperature gradient—the “interface”—can be regarded as a linear mean “front” with superimposed “meanders” of varying size. Often, for simplicity, such alongfront meander is ignored, and the resulting BL modification by the mean front is treated two-dimensionally. We employ a three-dimensional model to investigate the mesoscale influence of such meanders, vis-à-vis those of the mean front, on the BL near an idealized meandering front.

Strong surface temperature gradients often exist near surface interfaces, such as land–water and ice–water boundaries, and at sea surface temperature (SST) oceanic fronts. SST fronts develop meanders whose size and location change, often becoming especially convoluted in response to atmospheric storms (Stommel 1966). The associated meander length scales cover a wide range, from 30 km (Ramp et al. 1991) to 300 km (Mulhearn 1987), which may indicate scale separations produced by differing physical mechanisms.

Meanders of such differing sizes have differing mesoscale influences. To illustrate such differences, the effect of a large-scale meander of the SST gradient was readily apparent in the BL structure of the GALE IOP 2 (Genesis of Atlantic Lows Experiment Intensive Ob-

servations Period 2) simulation of Warner et al. (1990), but a smaller-scale meander exhibited little distinguishable effect in a similar simulation by Doyle and Warner (1993). We seek reasons for such differences and criteria predicting whether a meander imposes a signature upon the BL structure.

Specifically, we investigate the effect of meander scale relative to two internal atmospheric scales: a mesoscale deformation radius and an alongfront advective length scale. Dalu and Pielke (1993) have analytically investigated a related problem, the importance of the mesoscale circulation induced by one-dimensional periodic variations of surface heat flux. They found that the magnitude of the mesoscale vertical velocity and its associated heat flux decreased very slowly with increasing wavelength of the forcing heat flux when that wavelength was smaller than the deformation radius, but decreased more rapidly for larger wavelengths. Their two-dimensional model represented a series of discrete warm–cold surface patches and assumed the forcing to be periodic in time. In addition, linearization required by their analytic treatment did not allow investigation of advective effects, and they neglected large-scale wind forcing. The present numerical investigation considers the three-dimensional fields produced by a meandering warm–cold surface interface constant in time, as befits SST gradients, and explicitly examines the influence of a large-scale geostrophic wind, including advective effects.

To outline our investigation, the simulation model and parameters are described in section 2. Section 3 discusses the scaling lengths that characterize the results. Section 4 and section 5 illustrate response changes to meander of

Corresponding author address: Dr. John W. Glendening, Naval Research Laboratory, Code 7541, Monterey, CA 93943-5006.

differing scales with and without geostrophic forcing, respectively. Section 6 investigates the effect of strong alongfront advection. Section 7 extends the conclusions of previous sections to more general conditions. Section 8 demonstrates an application of these conclusions to less idealized conditions. Section 9 summarizes the investigation's conclusions.

We will demonstrate that the thermally induced circulation changes from, at large meander scales, a series of quasi-two-dimensional (2D) circulations oriented perpendicular to the local interface to become, at small meander scales, a quasi 2D circulation oriented perpendicular to the mean front. In interpreting our three-dimensional results, therefore, we utilize results from a 2D simulation obtained by Glendening [1994, abbreviated as 2D (G)]. For a given large-scale geostrophic windspeed G , the "optimal"—that is, largest—value of w_{max} (the domainwide maximum of vertical velocity) produced by a surface temperature interface occurs at geostrophic angles where the BL "headwind" produced by frictional modification of the geostrophic wind most effectively "counterbalances" thermally induced flow at the interface. This produces vertically averaged BL winds paralleling the surface interface near the interface and consequent strong gradients. Figure 1 illustrates this for $G = 10 \text{ m s}^{-1}$ and parameters specified in section 2, with w_{opt} occurring at angle ϕ_{opt} . Greater (smaller) angles produce headwinds greater (smaller) than optimal, increasing the cross-interface advection and reducing boundary-layer (BL) gradients. As illustrated, the two optimal geostrophic directions have differing cross-interface angles and w_{opt} values due to asymmetry introduced by surface friction. Here ϕ_{opt} depends upon the vertical stress divergence through the BL near the interface, a function of the average surface roughness and BL depth, whereas w_{opt} depends upon differences in BL stress divergence between the warm and cold surfaces.

2. Experimental design and model description

The surface temperature interface is idealized as a superposition of a linear mean "front" and a sinusoidal

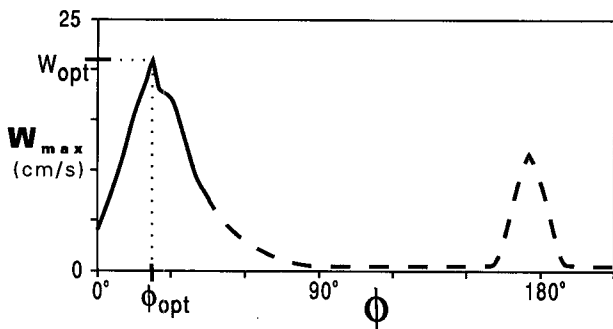


FIG. 1. Domain maximum vertical velocity (w_{max}) as a function of geostrophic angle (ϕ) for two-dimensional simulations with $G = 10 \text{ m s}^{-1}$. Dashed line indicates expected asymmetry of southerly geostrophic winds, based upon Glendening (1994).

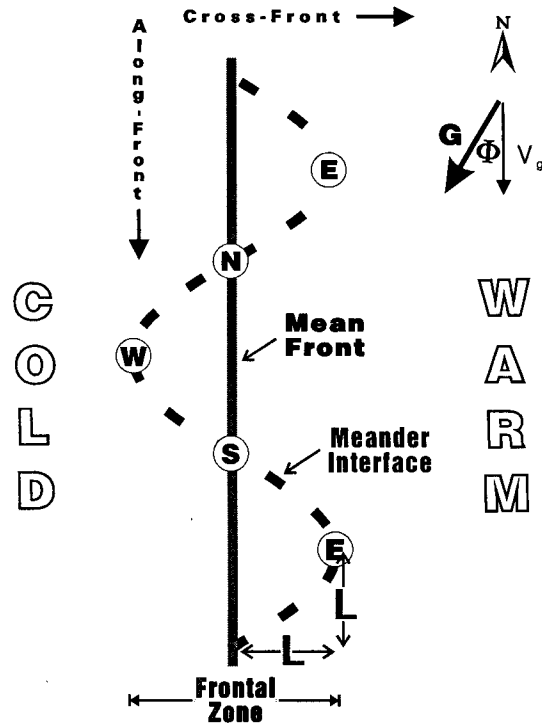


FIG. 2. Idealized mean front with sinusoidal meander.

alongfront "meander," as shown in Fig. 2. Here front describes the *mean* front, oriented in a north-south direction, about which the meander occurs, and interface describes local variations about the mean front. (Directions, such as north, refer to the assumed orientation of the mean front.) The scale of the meander is represented by L , which equals both the amplitude and quarter-wavelength of the sinusoid. The "meander ratio"—the ratio between the cross- and alongaxis scales—thus equals 1. The term "frontal zone" describes the region extending a distance L to each side of the mean front. Location identifiers W and E indicate positions near the two vertices, representing the cold and warm sides of the mean frontal zone, respectively, where the local interface approximately parallels the mean front. Identifiers N and S indicate intermediate regions, where the interface is least parallel to the mean front. The geostrophic wind, here referring to a large-scale forcing not to a locally varying pressure gradient, has magnitude G oriented at angle Φ to the mean front.

The simulations employ the atmospheric portion of the U.S. Navy's Coupled Ocean Atmosphere Mesoscale Prediction System (COAMPS), which solves fully compressible equations of motion (Hodur 1993). Vertical mixing results from predicted turbulent kinetic energy (TKE) (Therry and Lacarrère 1983), the assumed BL top occurring where the TKE drops to 20% of its profile maximum. To focus on the fundamental atmospheric response to surface temperature meander,

a dry version avoids complications associated with moisture and latent heat release. The lateral boundaries are periodic in y and open in x . The latter permit outward propagation of gravity waves and are placed at least one, and as much as two, deformation radii from the frontal zone. The horizontal grid increment is 5 km, except as discussed in section 6. The vertically stretched 35-level grid employs 20 levels in the lowest 2 km to resolve the lower-tropospheric response.

Idealized simulation parameters are based on GALE IOP2 (Doyle and Warner 1993). Initial potential temperatures are horizontally homogeneous with $\Gamma \equiv \partial\theta/\partial z = 5 \text{ K km}^{-1}$. Prescribed surface temperatures are 14°C over the cold surface and 22°C over the warm surface. The Coriolis parameter, f , is $7.29 \times 10^{-5} \text{ s}^{-1}$, a value appropriate to 30°N . Simulations are run with $L = 20, 27, 40, 60, 80, 120, 180,$ and 240 km for $G = 0$ and 10 m s^{-1} and with $L = 75, 150, 240, 300, 600,$ and 1200 km for $G = 30 \text{ m s}^{-1}$. All simulations are integrated to a quasi-stationary state at 48 hours after initialization. As one measure of stationarity, the domain maximum vertical velocity typically changes by 1%–10% over the final 6 hours.

3. Alongfront scaling lengths

The fundamental horizontal length scale governing geostrophic adjustment between boundary layers over two surfaces of differing temperature, for which advection is solely self-induced by BL thermal forcing, is the mesoscale deformation radius R . When a well-mixed BL results, R represents the distance that the equilibrium jet, which reflects the maximum horizontal gradient of mass or temperature, is displaced by advection from the interface (Glendening 1993). Thus, R controls the horizontal extent influenced by self-induced circulations. For geostrophic adjustment under stationary forcing, R can be estimated from

$$R \approx \frac{6ND_w}{7\pi f}, \quad (1)$$

where D_w is the BL depth over the warmer surface and $N \equiv [g\Gamma/\Theta_0]^{1/2}$ is the Brunt–Väisälä frequency (Glendening 1993). Rotunno (1983) has demonstrated a related linear dependence upon the mesoscale deformation radius for transient forcing by a sea breeze. The parameter indicating the dependence on alongfront variations, relating the scale of the meander to the scale of geostrophic adjustment, is therefore L/R .

Superimposing a large-scale geostrophic forcing on this adjustment introduces an additional length scale, the advective length scale parallel to the front. This length scale is the product of the characteristic time over which this advection is significant, the geostrophic adjustment scale f^{-1} (Blumen 1967), and the characteristic velocity parallel to the front. While BL advection depends upon the frictionally modified BL velocity, its a priori estimation can be difficult, so we neglect

this scaling complication and utilize the geostrophic component parallel to the front, V_g , to characterize the alongfront length scale

$$\Lambda \equiv \frac{V_g}{f}. \quad (2)$$

Parameter L/Λ indicates the importance of large-scale advection for alongfront variations. Over land surfaces friction is more significant and a frictionally modified alongfront velocity may better define this advective scale. Note that Λ is proportional to R divided by an atmospheric Froude number ND_w/V_g .

Parameter L/Λ obviously represents a dependence upon alongfront advection, but parameter L/R can also be viewed as representing such a dependence. For nonlinear geostrophic adjustment of a well-mixed layer, the alongfront jet that develops has magnitude

$$V_{\max} = fR \quad (3)$$

(Glendening 1993) for ideal conditions that neglect the effect of BL friction and mixing. Parameter L/R thus equals Lf/V_{\max} , reflecting a dependence upon alongfront advection produced by self-induced thermal forcing. However, velocity scale V_g in L/Λ represents a domainwide advection while velocity scale V_{\max} is a local jet maximum, larger than the area average of the varying thermally induced alongfront velocities.

4. Effect of self-induced thermal forcing

This section investigates dependence upon meander scale in the absence of alongfront advection imposed by a large-scale forcing. Advection is then self-induced by thermal forcing within the BL, and the horizontal scaling length is the mesoscale deformation radius R created by BL forcing. The associated 2D w_{\max} is not optimal, as no geostrophic wind exists to produce the required head wind. The warm-side BL depth, $D_w \approx 1300 \text{ m}$, with (1) gives $R \approx 65 \text{ km}$.

a. Large-scale meander

Large-scale alongfront variations are represented by our largest meander scale length $L = 240 \text{ km}$, so $L/R \approx 4$. Because $L/R \gg 1$, adjustments created by temperature differences across the interface act relatively independently across each local interfacial section. The resulting fields largely resemble those obtained by a 2D simulation oriented perpendicular to each local interface, somewhat modified by interactions created by the sinusoidal variation of the interface.

Figure 3a depicts w at $z = 500 \text{ m}$, approximately the midlevel of the warm-side BL. A line of maximum upward motion parallels the interface, displaced into the warm-side BL by thermally induced cross-interface flow. Generally varying between 2 and 4 cm s^{-1} , these maxima encompass the $3\frac{1}{2} \text{ cm s}^{-1}$ maximum produced by a true 2D simulation.

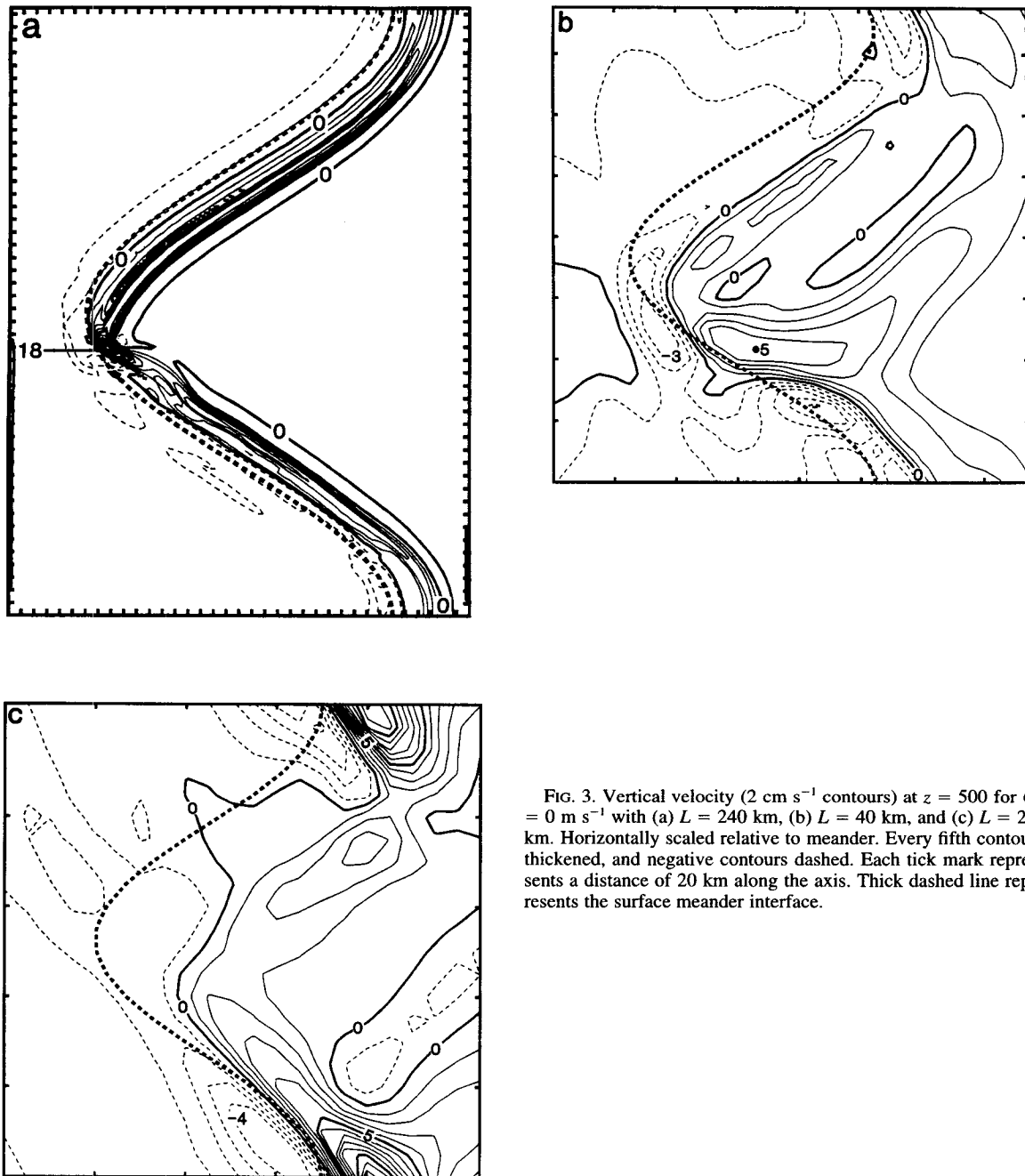


FIG. 3. Vertical velocity (2 cm s^{-1} contours) at $z = 500$ for $G = 0 \text{ m s}^{-1}$ with (a) $L = 240 \text{ km}$, (b) $L = 40 \text{ km}$, and (c) $L = 27 \text{ km}$. Horizontally scaled relative to meander. Every fifth contour thickened, and negative contours dashed. Each tick mark represents a distance of 20 km along the axis. Thick dashed line represents the surface meander interface.

Superimposed along-interface variations produce convergence (divergence) near vertex W (E). The localized maximum of 18 cm s^{-1} is displaced southward from the center of geometric dispersion by advection created by Coriolis turning. Self-induced alongfront advection thus creates asymmetry and strengthens the updraft maximum. If the alongfront velocity, v , were constant with increasing distance from vertex W along in-

terface S, the change in interface orientation would increase the effective "headwind." However, v instead becomes less negative (i.e., the alongfront component opposing the thermally induced flow decreases, see Fig. 4a), which acts to decrease the effective head wind. These opposing tendencies yield a w maximum displaced from vertex W by 60 km , roughly equal to R.

Boundary-layer temperature gradients approxi-

mately parallel the interface, as reflected in the BL depths (Fig. 5a). The BL grows over the warm side, with slightly smaller (larger) depth gradients for locations near N (S) due to induced cross-front advection.

Velocity jets created by geostrophic adjustment likewise parallel the interface, a northerly jet within the warm-side BL and a complementary southerly jet above the cold-side BL (Fig. 6). Advection resulting from geostrophic adjustment displaces the southerly jet from the interface by a distance R at the vertices, with

additional geostrophic advection producing larger (smaller) displacements near S (N).

Boundary-layer wind vectors and v isopleths are shown in Fig. 4a for $z = 65$ m, a level near the middle of the cold-side BL, which also represents winds within the warm-side BL since the latter is relatively well mixed. Thermal forcing strengthens (weakens) v near interface N (S).

The w maximum near vertex W, a departure from the overall two-dimensionality perpendicular to the interface, significantly impacts the local circulation. Fig-

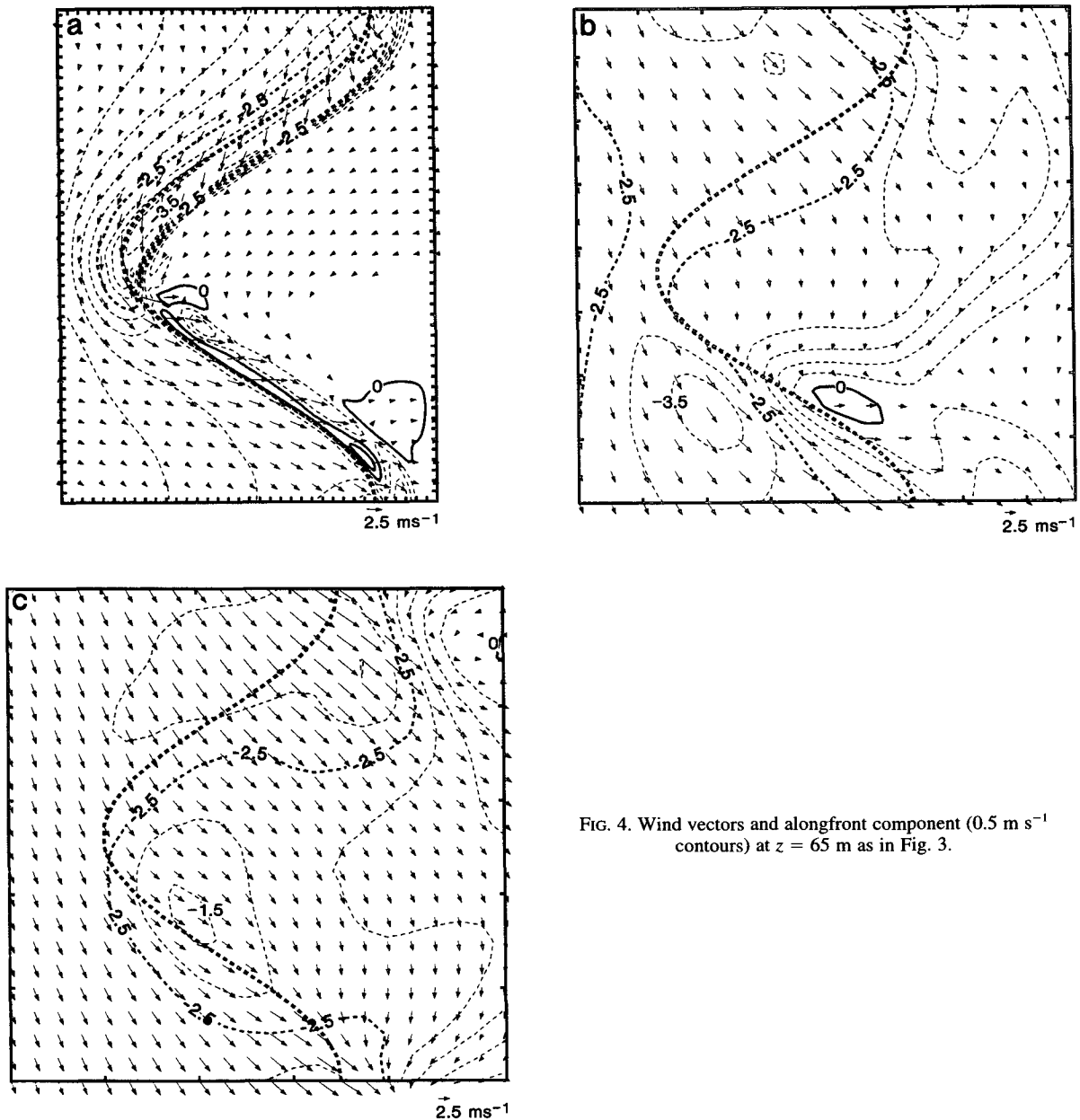


FIG. 4. Wind vectors and alongfront component (0.5 m s^{-1} contours) at $z = 65$ m as in Fig. 3.

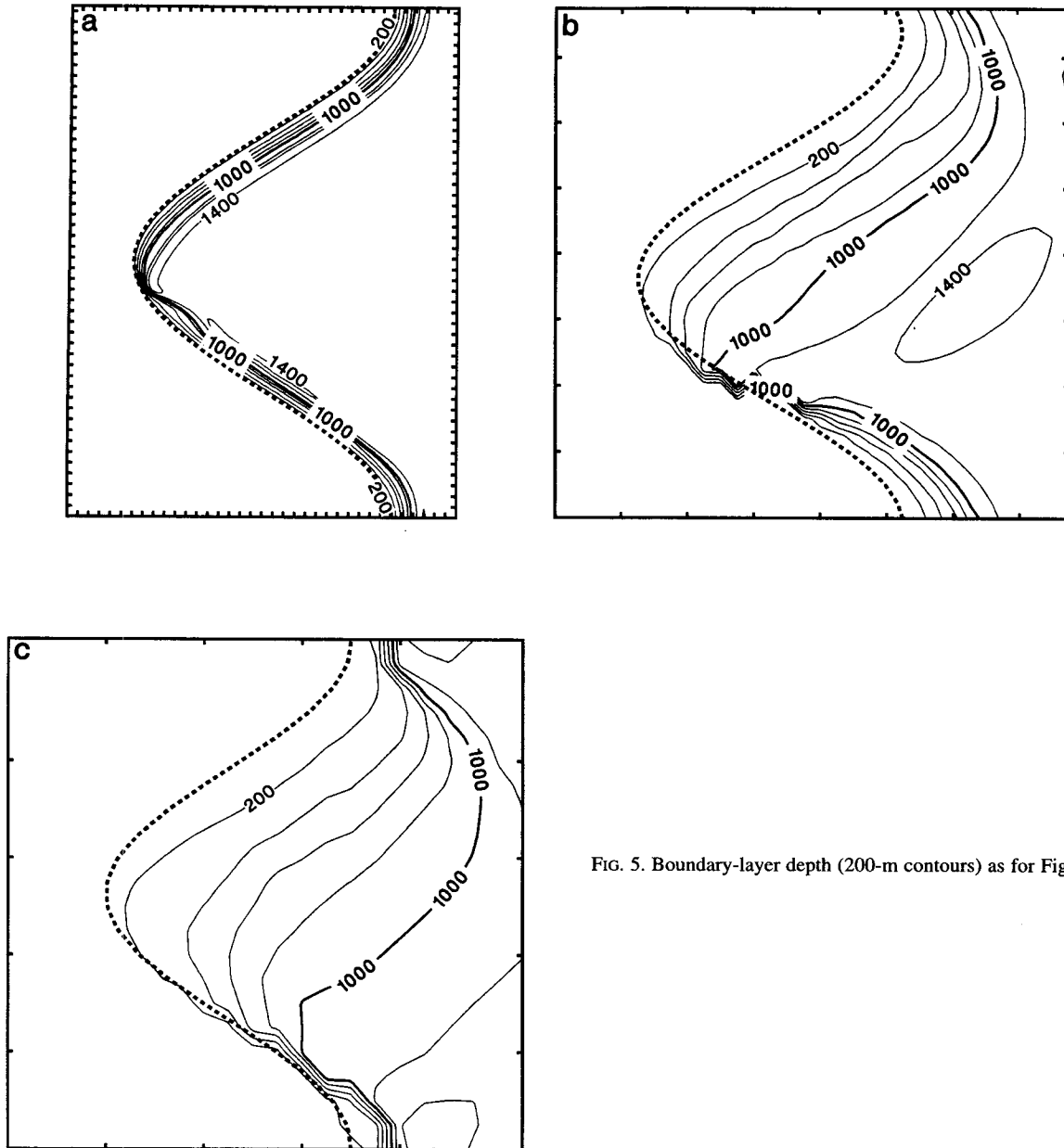


FIG. 5. Boundary-layer depth (200-m contours) as for Fig. 3.

ure 7 provides a detailed view of this feature, evincing the counterbalancing that produces BL winds nearly parallel to the interface near the w maximum and allows a strong temperature gradient to form. This maximum must become smaller for meander of larger scale, as the fields more nearly approach 2D circulations perpendicular to the local interface.

b. Intermediate-scale meander

As the meander scale decreases, geometric convergence increases near vertex W. The velocity compo-

nent perpendicular to the interface, created by Coriolis turning of the thermally induced flow near vertex W, increases to produce an "optimal" headwind counterbalancing the thermally induced cross-interface component. The w maximum therefore develops closer to the interface and is strengthened (not shown).

For $L < R$, thermally induced adjustments interact laterally along each interfacial section. A "blended" region results, with gradients relatively more perpendicular to the mean front than to the local interface. Blending of the temperature gradients is reflected by

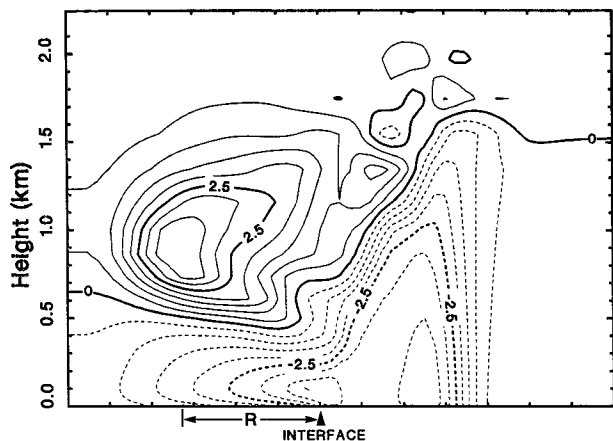


FIG. 6. Cross section of alongfront velocity (0.5 m s^{-1} contours) at vertex W for $G = 0$ with $L = 240 \text{ km}$.

the warm-side BL depth in Fig. 5b for $L = 40 \text{ km}$ ($L/R \approx 0.6$), with the 1000-m contour, for example, being pinched between the W vertices. The increasingly cross-frontal orientation is also apparent in the v contours (Fig. 4b). The overall cross-frontal flow produced by the developing quasi-2D mean front moves the position of maximum w eastward relative to the frontal zone, but its absolute distance from vertex W remains comparable to R (Fig. 3b).

c. Small-scale meander

For $L \ll R$, gradients become oriented perpendicular to the mean front rather than to the interface. In Fig. 3c, for $L = 27 \text{ km}$ so $L/R \approx 0.4$, the w maximum has migrated to vertex E. This results from alongfront blending, since in 2D(G) the w maximum occurs near the warm edge of a finite-width transition zone. Alternatively, this may be viewed as geostrophic adjustment acting to produce a w maximum at an approximate distance R from vertex W, which moves it eastward relative to the sinusoidal interface. As the scale decreases further, the w maximum moves south of vertex E and elongates to become a more linear feature paralleling the front (not shown).

The overall alongfrontal orientation of the thermal structure, modified by the local interface, is apparent in contours of the BL depth (Fig. 5c). Coriolis turning of the blended cross-frontal thermal forcing flow produces northwesterly BL flow over nearly the entire domain (Fig. 4c), and the southerly jet above the cold-side BL is essentially a linear feature, paralleling the mean front and offset laterally from it—vice from the interface for $L = 240 \text{ km}$ —by approximately R (not shown).

d. Overall dependence upon scale

Figure 8 depicts the scale dependence of the domain maximum w , w_{max} , which typically occurs near the BL

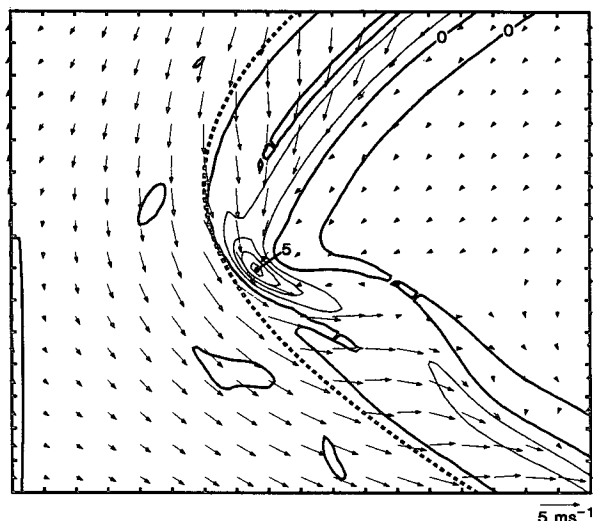


FIG. 7. Vertical velocity (1 cm s^{-1} contours) and horizontal velocity vectors for $G = 0 \text{ m s}^{-1}$ at $z = 65 \text{ m}$ with $L = 240 \text{ km}$.

top, and summarizes variations with meander scale using additional runs not discussed above. For $L \gg R$, w_{max} approaches the 2D w_{max} since local circulations are quasi 2D perpendicular to the meandering interface. At smaller meander scales, three-dimensional effects become significant: the ‘‘headwind’’ produced by local interface variation strengthens w_{max} , producing a maximum at $L/R \approx 2$ for our parameters. For $L < R$, increasing alongfront blending elongates the w maximum eastward, producing a relative minimum at $L/R \approx 0.6$. For smaller scales and further blending, w_{max} becomes established at the warm end of the frontal zone and increases until $L/R \approx 0.4$. At even smaller scales, although our grid resolution does not allow us to simulate them, alongfront variations must become fully blended to approach a quasi-2D mean front, with a line of maximum w paralleling the mean front as w_{max} decreases

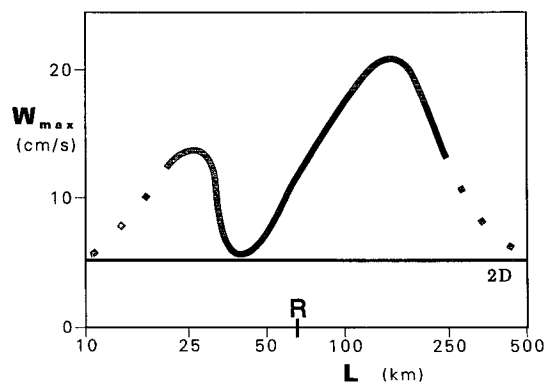


FIG. 8. Scale dependence for domain maxima of vertical motion for $G = 0 \text{ m s}^{-1}$. Dots extrapolate to two-dimensional limit indicated by horizontal line; R indicates deformation radius.

to its 2D value. The change with scale of w_{\max} is somewhat complex, but the transition centers around $L/R \approx 1$, demonstrating that R is the appropriate characteristic length scale.

The magnitude of the domain v maximum, in contrast, remains approximately equal for all meander scales. This follows from (3). Its location, however, does change with scale.

5. Effect of large-scale forcing

This section imposes a large-scale geostrophic wind upon previous conditions, producing additional along-front advection. The chosen geostrophic wind direction is the “optimal” 2D angle, that is, that producing the largest w_{\max} for a 2D front. Using $G = 10 \text{ m s}^{-1}$, $\phi_{\text{opt}} = 22\frac{1}{2}^\circ$ and $w_{\text{opt}} = 21 \text{ cm s}^{-1}$ (see Fig. 1). Choosing $\Phi = \phi_{\text{opt}}$ investigates conditions producing a strong response in vertical motion with, as will be demonstrated, equal large- and small-scale limits and is within the range of observed GALE IOP2 conditions. Warm-side BL depths are slightly deeper than in section 4, due to additional shear production of TKE, so R increases to 90 km. The additional length scale introduced by alongfront geostrophic advection, Λ , is 125 km.

a. Large-scale meander

Alongfront variations of large scale are illustrated by $L = 240 \text{ km}$, so $L/R \approx 3$ and $L/\Lambda \approx 2$. Overall, the fields are quasi-2D circulations oriented perpendicular to the local interface, slightly modified by their neighboring circulations. The geostrophic wind angle varies relative to the interface, so w maxima occur near vertices E and W (Fig. 9a), where the local geostrophic angle equals ϕ_{opt} . There the BL velocity approximately parallels the interface, evincing counterbalancing of the thermally induced flow by frictional turning of the geostrophic wind (Fig. 10a). Both w maxima are displaced from the vertex by a distance roughly equal to R . The maximum near vertex E —termed “Maximum I”—is displaced directly southward and elongated by the BL velocity advection. The maximum near vertex W —“Maximum II”—is displaced and elongated along the interface, partially reflecting the turning of winds to parallel the interface, as occurred for the “ $G = 0$ ” case.

Largest thermal gradients occur near the vertices due to the relatively small cross-interface advection there, as reflected in large BL depth gradients (Fig. 11a). The steep BL depth gradient is advected south from interface N , while along interface S the BL depth changes discontinuously to that of the cold-side BL, with overriding residual warm-side BL air. Rotation from the geostrophic angle is largest in the cold-side BL, since its smaller BL depth produces greater stress divergence, while near the interface the vectors are rotated counterclockwise by the thermally induced cross-interface flow.

b. Intermediate-scale meander

As L approaches R , Maxima I and II both decrease in magnitude, particularly the latter (not shown). Their absolute distance from each vertex remains comparable to R , so the relative distances increase.

For $L < R$, Maximum II becomes considerably weaker than Maximum I, as depicted in Fig. 9b with $L = 60 \text{ km}$, so $L/R \approx 0.7$ and $L/\Lambda \approx 0.5$. A convergence line extends from vertex E downstream (with respect to the BL wind) to interface S , produced by frictional differences between air relatively unaffected by the cold surface, to the east of the line and the larger counterclockwise rotation produced by stronger stress divergence in the cold-side BL. This produces a new maximum—“Maximum III”—downstream of Maximum I: as the warm-side BL air reaches interface S , additional BL friction reduces the component perpendicular to the interface, creating convergence in the cold-side BL that strengthens preexisting upward motion in the warm-side air to produce a w maximum near the middle of the overriding warm layer. Lateral blending from geostrophic adjustment is now more significant, as reflected in greater north–south orientation of contours of BL depth (Fig. 11b) and v (Fig. 10b).

c. Small-scale meander

For $L \ll R$, adjustment blending creates a quasi-2D front parallel to the mean front over a transition zone of width $2L$. Figure 9c illustrates this for $L = 27 \text{ km}$, so $L/R \approx 0.3$ and $L/\Lambda \approx 0.2$. Since $\Phi = \phi_{\text{opt}}$, the magnitudes of maxima I and III increase toward w_{opt} . They eventually blend into a line along the warm end of the frontal zone, where the wind is most parallel to the mean front, as for a finite-width transition zone in 2D(G). Maximum II diminishes and eventually vanishes. Contours of BL temperature (not shown), BL depth (Fig. 11c), and v (Fig. 10c) largely parallel the mean front. Other 2D mean frontal features include BL wind confluence toward the frontal zone, partly resulting from stress divergence between the warm- and cold-side BLs and partly from the thermally induced component, and a v maximum resulting from Coriolis turning of the thermally induced pressure gradient.

d. Overall dependence upon scale

For these simulations, R and Λ are comparable and the transition from alongfront sinusoidal variation to alongfront blending occurs for L near both R and Λ . Effects of geostrophically induced alongfront advection are evident; with $L = 27 \text{ km}$, for example, w and BL depth gradients show less alongfront variation than for the $G = 0$ case.

Figure 12 displays w_{\max} , using additional runs not discussed above, to summarize the effects of meander scale. At largest scales, the local circulations are quasi-2D perpendicular to the meandering interface, so max-

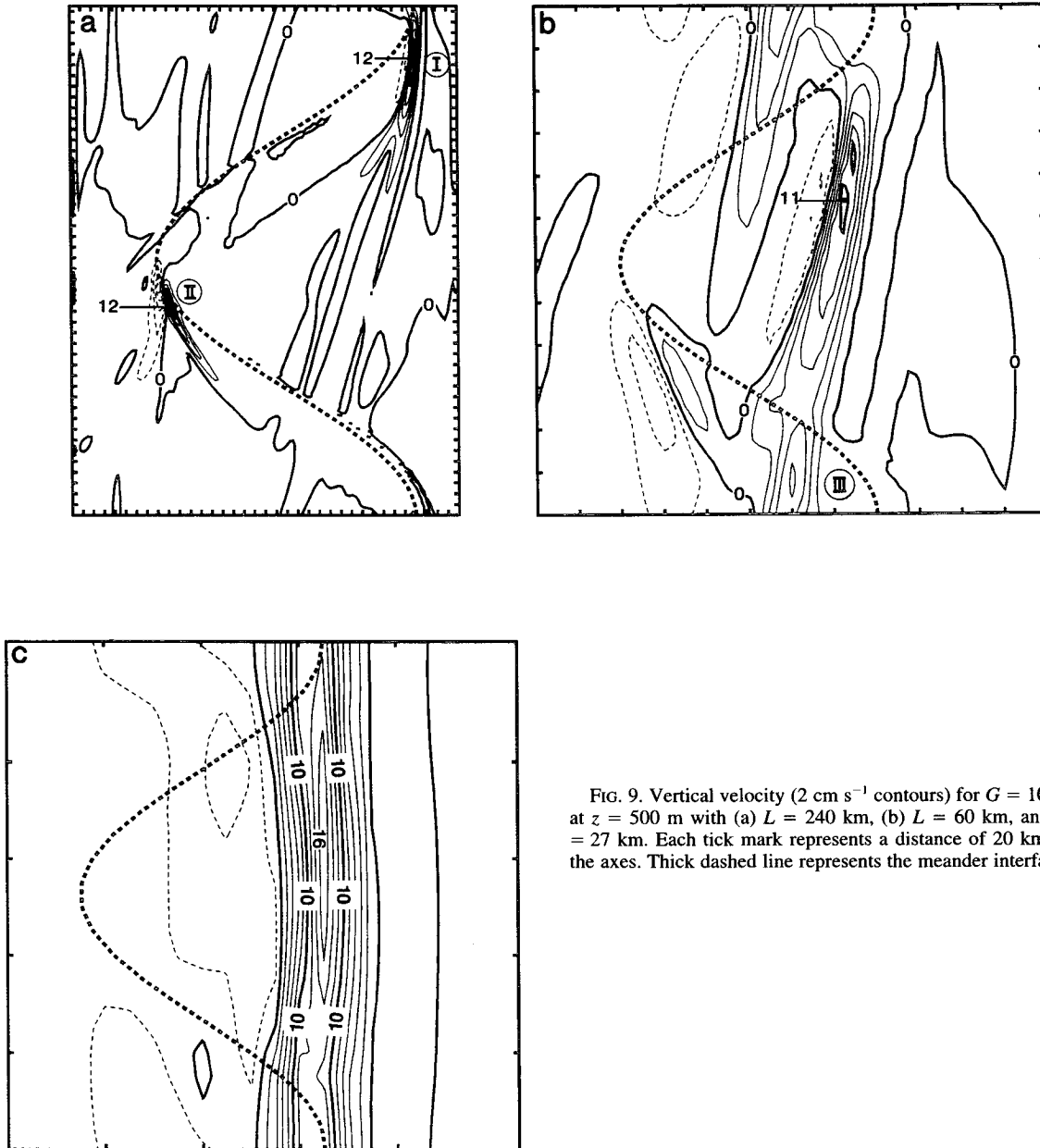


FIG. 9. Vertical velocity (2 cm s^{-1} contours) for $G = 10 \text{ m s}^{-1}$ at $z = 500 \text{ m}$ with (a) $L = 240 \text{ km}$, (b) $L = 60 \text{ km}$, and (c) $L = 27 \text{ km}$. Each tick mark represents a distance of 20 km along the axes. Thick dashed line represents the meander interface.

ima I and II approach the 2D limit and, since $\Phi = \phi_{\text{opt}}$, develop near the two vertices. As L is reduced, three-dimensional effects become important and both maxima diminish while Maximum III develops. At smallest scales, Maxima I and III merge into a single maximum, which equals w_{opt} since $\Phi = \phi_{\text{opt}}$. Both the lowest value of Maximum I and the point of equal w_{max} of Maxima II and III occur near R (and Λ), characterizing it as a midpoint between the large- and small-scale limits. The relative symmetry of the w_{max} variation results from choosing $\Phi = \phi_{\text{opt}}$. For other geostrophic angles, w_{max}

exhibits an asymmetric dependence upon L , as the next section demonstrates.

6. Effect of strong alongfront advection

In this section we increase the alongfront geostrophic advection to make $\Lambda \gg R$ and choose a nonoptimal geostrophic angle to illustrate scale variations under more general wind directions. We choose $G = 30 \text{ m s}^{-1}$ and $\Phi = 71/2^\circ$, so the large-scale front-normal component approximately equals that of section 5. The BL

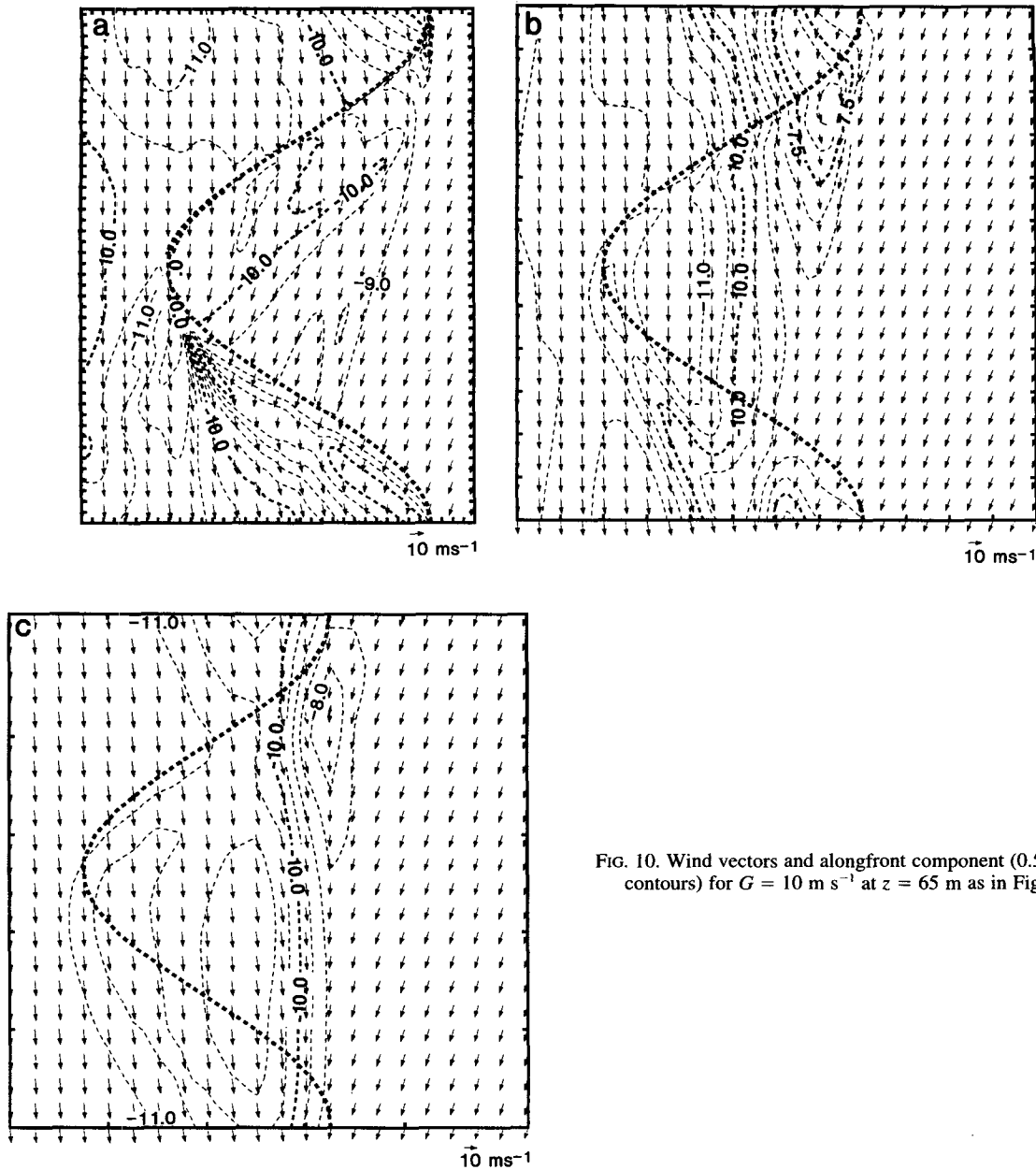


FIG. 10. Wind vectors and alongfront component (0.5 m s^{-1} contours) for $G = 10 \text{ m s}^{-1}$ at $z = 65 \text{ m}$ as in Fig. 9.

front-normal components differ, however, and the 2D w_{opt} of 6.9 m s^{-1} occurs at $\phi_{\text{opt}} = 171\frac{1}{2}^\circ$; Λ increases to 410 km and warm-side BL depths increase slightly, so $R = 100 \text{ km}$. The scales investigated are considerably larger than in previous sections, necessitating a fivefold increase in horizontal grid spacing to 25 km. The resulting vertical velocities are greatly reduced, vitiating quantitative comparisons with previous sections.

Figure 13 summarizes meander scale effects. For the largest scale simulated, the circulations are quasi 2D perpendicular to the local interface. Two w_{max} result, shifted from the vertices towards the midpoint of interface S to positions where the local geostrophic angle

approximately equals ϕ_{opt} . The circulations are not fully two-dimensional, so quantitatively the maxima are smaller than w_{opt} , but at larger scales they must approach w_{opt} . Maximum II, the maximum closer to the cold side, is slightly stronger than Maximum I. As L decreases, Maximum II moves eastward and Maximum I migrates south of vertex E, along interface N, while their magnitudes fluctuate. For $L \ll R$, alongfront blending dominates and only a single maximum remains, located on the warm side of the mean front. Its magnitude approaches the 2D value for that geostrophic angle, a magnitude smaller than w_{opt} since $\Phi \neq \phi_{\text{opt}}$.

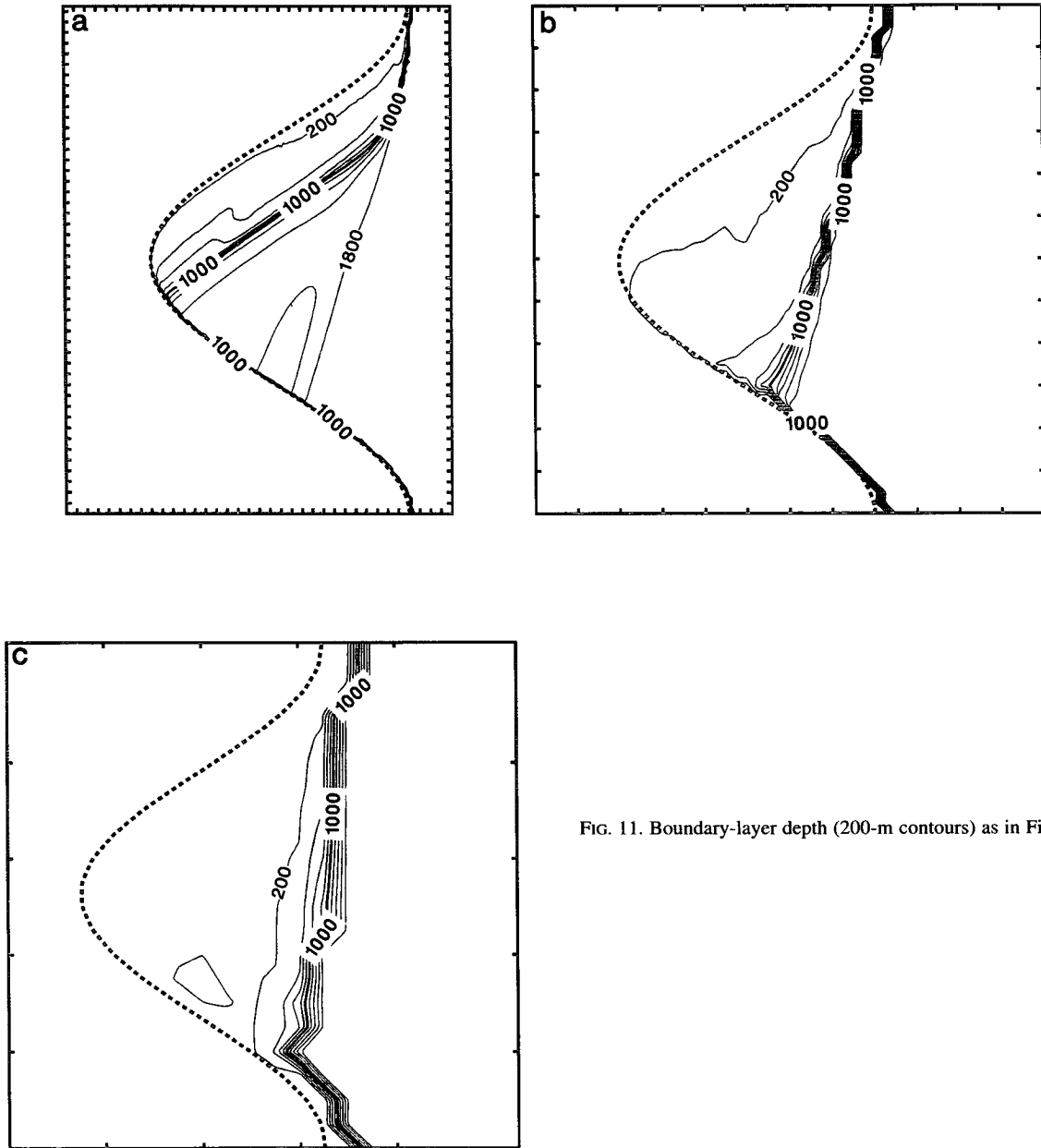


FIG. 11. Boundary-layer depth (200-m contours) as in Fig. 9.

Figure 13 demonstrates that strong alongfront geostrophic advection lowers w_{\max} below w_{opt} unless $L \gg \Lambda$. Such advection does not, however, produce alongfront blending, which requires $L \ll R$. Thus, R controls the approach to the small-scale limit, whereas Λ controls the approach to the large-scale limit when $\Lambda > R$.

7. Extension to generalized conditions

The preceding sections demonstrate scale dependence upon parameters L/R and L/Λ for three selected

cases of G and Φ . We now extend these ideas to consider scale dependence under more general conditions of G and Φ . Figure 14 illustrates this dependence based upon the following discussion.

For meander of smallest scale, $L \ll R$, the circulation is quasi 2D oriented perpendicular to the mean front. A single domain maximum vertical velocity, w_{\max} , develops on the warm side of the frontal zone, with magnitude equal to that of a 2D circulation with a geostrophic angle of Φ and varying with G and Φ just as a 2D circulation w_{\max} varies with G and ϕ (e.g., Fig. 1).

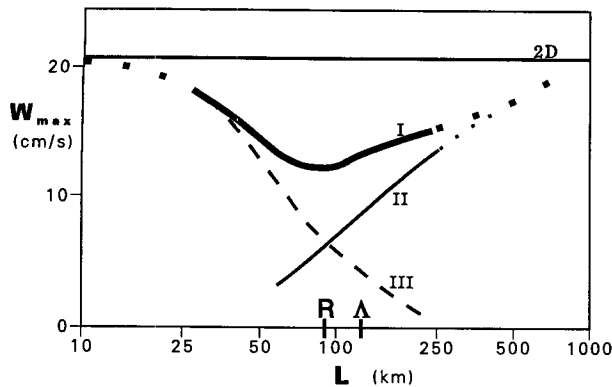


FIG. 12. Scale dependence for domain maxima of vertical motion for $G = 10 \text{ m s}^{-1}$ for Maxima I (thick solid), II (thin solid), and III (dash). Dots extrapolate to two-dimensional limit indicated by horizontal line; R indicates deformation radius; Δ indicates alongfront geostrophic advection scale.

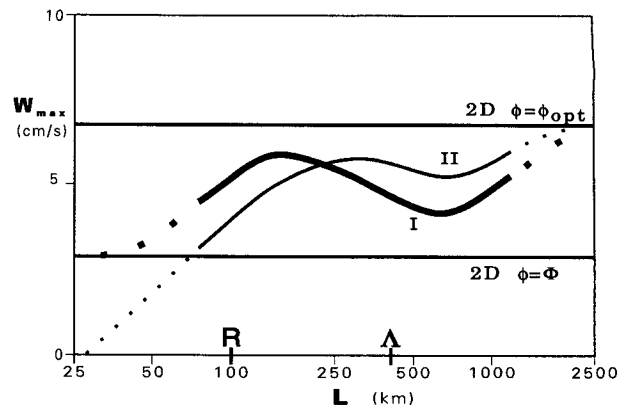


FIG. 13. Scale dependence for domain maxima of vertical motion for $G = 30 \text{ m s}^{-1}$ for Maxima I (thick solid) and II (thin solid). Dots extrapolate to two-dimensional limits indicated by horizontal lines; R indicates deformation radius; Δ indicates alongfront geostrophic advection scale.

The small-scale w_{max} is thus largest when Φ equals ϕ_{opt} , as indicated by the upward-pointing arrow in Fig. 14.

Transition from small to intermediate scale occurs as L increases towards R , weakening the adjustment blending and developing an additional w_{max} to the cold-side of the existing maximum. The positions and magnitudes of the maxima vary with changes in the self-induced (by geostrophic adjustment) or externally induced (by the large-scale geostrophic wind) alongfront advection.

Changes at intermediate scales are especially complex when geostrophically induced velocities are small relative to thermally induced velocities, that is, for $G \ll fR$, as nonlinearities created by geometric variation of the local thermally induced headwind become significant. The largest w_{max} then develops at intermediate scales, not at the large-scale limit, as demonstrated by the “ $G = 0$ ” simulations (Fig. 8). The shaded line in Fig. 14 indicates this possible complexity.

For meander of largest scale, $L \gg \max[R, \Delta]$, the fields approach quasi-2D circulations perpendicular to the local interface and both w maxima approach the same value. The local angle variation created by the meandering interface produces a series of local 2D circulations with effective 2D geostrophic angles covering the range $\Phi \pm \Delta\phi$. The angular range $\Delta\phi$ depends upon the meander ratio and shape of the meander; for example, $\Delta\phi = \pm 58^\circ$ for our sinusoidal meander ratio of 1. Two local geostrophic angles produce a w_{max} . For Φ within the range $\phi_{\text{opt}} \pm \Delta\phi$, $w_{\text{max}} \approx w_{\text{opt}}$. The large-scale limit w_{max} is thus robust to changes in Φ . The location of the maxima vary, however, occurring where the local geostrophic angles equal ϕ_{opt} . For Φ outside this range, the large-scale w_{max} is smaller than w_{opt} but still larger than the small-scale w_{max} . So long as G is sufficiently large that its frictionally modified BL velocity can effectively counter the thermally induced circulation, the largest w_{max} occurs at the large-scale

limit. Such is not true for smaller G , however, which reduces the large-scale w_{max} as indicated by the downward-pointing arrow in Fig. 14.

8. Discussion

The principles of the preceding section explain the dissimilar influences of SST meanders of differing scale noted in the introduction. For example, in Warner et al. (1990), a prominent SST meander eddy occurred near 35°N , 69°W , with a scale of approximately 90 km (based upon an estimated quarter-wavelength of 75 km and amplitude of 100 km), and its signature appeared in the vertical motion field (their Fig. 6). The GALE IOP2 parameters of section 2 apply. Warner et al. utilized no geostrophic velocity, so $R \approx 65 \text{ km}$ (section 4). Thus $L > R$, so the meander is not sufficiently small scale to produce lateral blending. In Doyle and

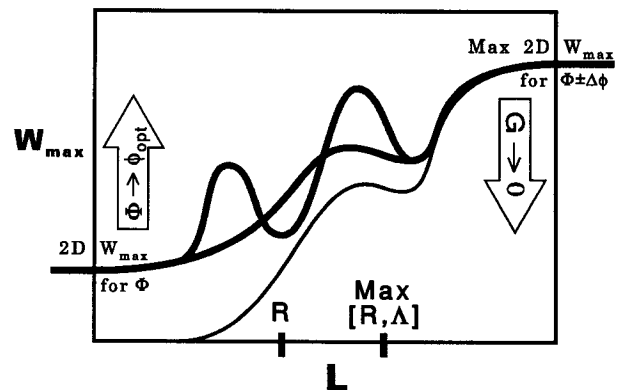


FIG. 14. Scale dependence under generalized conditions of geostrophic wind velocity and direction for vertical velocity maxima near the warm (thick line) and cold (thin line) side of frontal zone, as discussed in section 7.

Warner (1993), however, a distinct SST meander near 33°N, 78°W had a scale of 23 km (based upon an estimated quarter-wavelength of 25 km and an amplitude of 20 km), but no such signature appeared in the streamlines or in the vertical velocity field. They included a geostrophic wind of roughly 10 m s^{-1} , so $R \approx 90 \text{ km}$ (section 5). Thus $L \ll R$, so the meander is relatively small scale, significant lateral blending results, and no SST signature appears in the BL fields.

The dependence upon f implied by its inclusion in both R and Λ has been tested by increasing and decreasing f by a factor of 3 for $G = 10 \text{ m s}^{-1}$ with $L = 80 \text{ km}$. The qualitative changes follow those expected from consequent changes in R and Λ . For $3f$, as L/R increases, the magnitude of Maximum III is much smaller than that of Maxima I and II; also, Maximum II moves toward the cold side of the transition zone, its distance from vertex W being halved. For $f/3$, as L/R decreases, Maximum II disappears while Maxima I and II blend together to produce a line of maximum w along the warm edge of frontal zone (these cases were run to hour 72). However, this scaling is not exact: for $3f$ the resulting fields exhibit less blending than those for $L = 3 \times 80 \text{ km} = 240 \text{ km}$ with the reference f , whereas for $f/3$ the patterns display more blending than those for $L = 80 \text{ km}/3 = 27 \text{ km}$.

The geostrophic adjustment assumptions inherent in R and Λ are applicable at midlatitudes. The $f/3$ case strains this applicability, for at low latitudes additional scales must become important as R and Λ lose their relevance. For example, a reviewer notes the probable significance at small f of a length scale representing the growth of an internal BL. At midlatitudes, the quasi-equilibrium ageostrophic flow across mass contours is small since it depends upon surface fluxes and the heat flux is small over most of the domain after the atmosphere has adjusted to the constant surface temperature. There, an internal BL growth scale is apparently of minor importance, as tested—within a limited parameter space, for $L = 80$ and 100 km with $G = 10 \text{ m s}^{-1}$ —by additional runs using a halved surface heat flux: w is quantitatively reduced since it results from flow across the mass contours, but neither the BL depth nor the v component nor the qualitative dependence of w upon x , y , or L is significantly altered. At lower latitudes, however, flow across mass contours is less constrained and such a length scale is likely important. Since our analysis is based upon geostrophic adjustment assumptions, we do not examine the lower latitude limit.

9. Conclusions

The effect of alongfront meander depends upon its scale L relative to characteristic atmospheric scales. The fundamental characteristic scale, produced by thermally induced adjustments, is the mesoscale deformation radius R , which depends upon the boundary-layer depth over the warm side of the front. With weak geo-

strophic forcing, R is the characteristic scale separating small- from large-scale meander. With strong geostrophic forcing, however, R only controls the approach to small-scale limit, while the approach to the large-scale limit is controlled by the advective length Λ .

For large-scale meander, the fields are quasi two-dimensional, oriented perpendicular to the local interface, and the BL contains signatures of the individual meander elements. Maxima of vertical velocity typically form at two locations. Jets created by the thermal forcing parallel the interface.

For small-scale meander, the signature of an individual meander is lost to alongfront blending, orienting gradients perpendicular to the mean front with little alongfront variation. A single maximum of vertical velocity results on the warm side of the frontal zone. Jets now parallel the mean front.

Transition between the two limits is affected by along-interface variations created by geostrophic adjustment and by frictionally modified BL advection resulting from large-scale geostrophic forcing. This transition is more complex with weaker geostrophic winds.

Vertical velocity maxima occur when the thermally induced cross-interface BL flow is counterbalanced by a BL “headwind,” either self-induced by a neighboring thermal circulation of differing orientation or imposed by frictional modification of a large-scale geostrophic forcing. For geostrophic wind speeds sufficiently strong to counterbalance the thermally induced forcing, large-scale meanders produce the strongest vertical velocities. The large-scale limit is then less sensitive to changes in the geostrophic angle than is the small-scale limit. With weak geostrophic winds, self-induced “headwinds” dominate and vertical velocity maxima are stronger at intermediate meander scales than at either limit.

While both R and Λ are measures of the relative importance of alongfront advection, when ratioed to L the two length scales act differently: R reflects geostrophic adjustment, which couples the momentum equations through their Coriolis terms and constrains the flow to approximately parallel mass field contours; Λ , in contrast, acts through the advection terms, which depend upon a velocity roughly constant over the domain and alter the mass and velocity fields similarly. Thus R controls the alongfront blending, while Λ simply distorts the thermally induced response.

One implication of these results is that predictions of scales larger than R should not be sensitive to meanders of a sea surface temperature front smaller than R , given a large-scale forcing quasi stationary over a period longer than a half-pendulum day, since such variations are laterally blended by geostrophic adjustment processes into a mean front. The required oceanic resolution depends upon the atmospheric BL height and large-scale stratification. This argument applies only to the scale of convolutions of the surface areas—that is, their respective sizes and heat fluxes are assumed un-

affected—and assumes that nonlinear small-scale interactions ignored by our simulations, such as cloud formation, are not significant. Dalu and Pielke (1993) similarly concluded from their linear analytic work that resolution of one-dimensional surface thermal inhomogeneity was unnecessary for forcing scales smaller than the deformation radius.

While we have used SST meander to illustrate the effect of alongfront variations in surface temperature, these results can also characterize other surface temperature variations, such as the meander of an ice edge or the meander of a shoreline for which the effect of the thermal land–sea contrast dominates that of surface roughness or terrain differences.

Acknowledgments. The support of the sponsor, Office of Naval Research (ONR), program element 0601153N, is gratefully acknowledged. Additional support for JDD was provided by ONR Coastal Meteorology ARI program element 0602704N. We thank Dr. Richard Hodur of NRL Monterey for helpful discussions concerning the numerical model. Computer support was provided by the Department of Defense High Performance Computing Center at the U.S. Army Waterways Experimental Station.

REFERENCES

- Blumen, W., 1967: On nonlinear geostrophic adjustment. *J. Atmos. Sci.*, **24**, 325–332.
- Dalu, G. A., and R. A. Pielke, 1993: Vertical heat fluxes generated by mesoscale atmospheric flow induced by thermal inhomogeneities in the PBL. *J. Atmos. Sci.*, **50**, 919–926.
- Doyle, J. D., and Warner, T. T., 1993: Nonhydrostatic simulations of coastal mesobeta-scale vortices and frontogenesis. *Mon. Wea. Rev.*, **121**, 3371–3392.
- Glendening, J. W., 1993: Nonlinear displacement of the geostrophic velocity jet created by mass imbalance. *J. Atmos. Sci.*, **50**, 1617–1628.
- , 1994: Dependence of boundary-layer structure near an ice-edge coastal front upon geostrophic wind direction. *J. Geophys. Res.*, **99**(D), 5569–5581.
- Hodur, R. M., 1993: Development and testing of the Coupled Ocean/Atmosphere Mesoscale Prediction System (COAMPS). NRL/MR/7533-93-7213, Naval Research Laboratory, 84 pp. [Available from the Naval Research Laboratory, Monterey, CA 93943-5502.]
- Mulhearn, P. J., 1987: Tasman Front: A study using satellite infrared imagery. *J. Phys. Oceanogr.*, **17**, 1148–1155.
- Ramp, S. R., P. F. Jessen, K. H. Brink, P. P. Niiler, F. L. Daggett, and J. S. Best, 1991: The physical structure of cold filaments near Point Arena, California, during June 1987. *J. Geophys. Res.*, **96**(C), 14 859–14 883.
- Rotunno, R., 1983: On the linear theory of the land and sea breeze. *J. Atmos. Sci.*, **40**, 1999–2009.
- Stommel, H., 1966: *The Gulf Stream, A Physical and Dynamical Description*. University of California Press, 280.
- Therry, G., and P. Lacarrère, 1983: Improving the eddy kinetic energy model for planetary boundary layer description. *Bound.-Layer Meteor.*, **25**, 63–88.
- Warner, T. T., M. N. Lakhtakia, J. D. Doyle, and R. A. Pearson, 1990: Marine atmospheric boundary-layer circulations forced by Gulf Stream surface temperature gradients. *Mon. Wea. Rev.*, **118**, 309–323.